Coastal Engineering 179 (2023) 104241

Contents lists available at ScienceDirect

Coastal Engineering

journal homepage: www.elsevier.com/locate/coastaleng

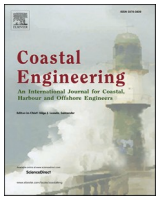

Comparison of deep-water-parameter-based wave overtopping with wirewall field measurements and social media reports at Crosby (UK)

Christopher H. Lashley [a,*], Jennifer M. Brown [b], Margaret J. Yelland [b,**], Jentsje W. van der Meer [c], Tim Pullen [d]

[a] Center for Applied Coastal Research, University of Delaware, Newark, DE, 19716, United States
[b] National Oceanography Centre, European Way, Southampton, SO14 3ZH, United Kingdom
[c] Van der Meer Consulting, P.O. Box 11, 8490 AA, Akkrum, the Netherlands
[d] HR Wallingford, Howbery Park, Wallingford, Oxfordshire, OX10, UK

ARTICLE INFO

Keywords:
Coastal hazard
Shallow foreshore
Parapet wall
Stepped revetment
Citizen science
Infragravity waves

ABSTRACT

Wave overtopping formulae, which often underlie coastal hazard early warning systems, are typically parameterised using wave conditions at the toe of the structure. For very shallow conditions where significant wave breaking occurs over the foreshore, this usually requires computationally-demanding numerical models—and practitioners skilled in their application—to accurately transform offshore waves to the structure toe. An additional concern is that overtopping formulae are scarcely validated in the field due to the very limited availability of in-situ overtopping data obtained at actual structures. Here, we validate a set of deep-water-parameter-based formulae for mean overtopping discharge (q) at smooth slopes, which remove the need for nearshore measurements or additional numerical modelling but require that a single representative foreshore slope angle (m) be defined. The validation is carried out against field data gathered at Crosby (UK) using two novel approaches: i) a new overtopping measurement system called "WireWall"; and ii) crowd-sourced data in the form of overtopping images obtained from a community Facebook page (social media). A method is introduced to define m for irregular bathymetries, based on the location where the local water depth is equal to the offshore significant wave height. The overtopping formulae proved accurate—with estimates of q being within a factor of 4 of observations—when compared to both 1-h averaged and 15-min averaged overtopping data, suggesting that the approach can be used for both design and assessment and now-casting hazard information. Finally, hindcasts made using the newly validated formulae for the events reported by the community indicate that q can exceed 10 l/s/m under yearly winter conditions, posing a serious hazard to pedestrians. This highlights the pressing need to update the current hazard warning system at Crosby, which estimates q to be a factor of 3 lower than the deep-water-parameter-based approach, on average.

1. Introduction

1.1. Background

In coastal hazard forecasting, practitioners must accurately estimate the volume of water that passes over sea defences due to wave action—referred to as wave overtopping—that may cause flooding, damage structures or injure people. This is often achieved using empirical formulae that relate wave conditions at the toe of the structure, and the structure's geometry, to a mean overtopping discharge, q (EurOtop, 2018). The main drawback to this approach lies in the fact that accurate wave measurements immediately in front of the structure are rarely available, compared to deep-water wave parameters which are often available via offshore buoys or reliable ocean-scale wave models (e.g., WaveWatch III (Tolman, 1999)). As a result, numerical models are typically used to transform wave conditions in deep water (offshore) to the structure toe.

The bathymetry seaward the structure (i.e. the foreshore) may be

* Corresponding author.
** Corresponding author.
E-mail addresses: clashley@udel.edu (C.H. Lashley), jebro@noc.ac.uk (J.M. Brown), m.yelland@noc.ac.uk (M.J. Yelland), jm@vandermeerconsulting.nl (J.W. van der Meer), t.pullen@hrwallingford.com (T. Pullen).

https://doi.org/10.1016/j.coastaleng.2022.104241
Received 11 August 2022; Received in revised form 6 September 2022; Accepted 15 October 2022
Available online 20 October 2022

classified by the relative water depth at the toe of the structure—defined as the ratio of the local water depth to the deep-water significant wave height ($h_{toe}/H_{m0,deep}$) (Hofland et al., 2017). For simple open coasts, with $h_{toe}/H_{m0,deep} > 1$, phase-averaged models (e.g. SWAN (Booij et al., 1999)) can quickly provide accurate estimates of wave conditions at the structure toe. However, for more shallow foreshores ($h_{toe}/H_{m0,deep} \leq 1$), phase-resolving wave models (e.g. XBeach (Roelvink et al., 2009) or FUNWAVE (Shi et al., 2012)) are needed to accurately capture the nonlinear effects of wave shoaling and breaking. This presents two challenges: first, because of their high computational demand, these models are generally impractical for large-scale applications; and second, such numerical models require practitioners with the specialized knowledge and skill to optimize their various parameters.

To overcome these challenges, Mase et al. (2013) proposed a set of deep-water-parameter-based formulae for seawalls with shallow foreshores. The formulae, which were later refined by Yuhi et al. (2021), directly relate wave run-up to overtopping and make use of an imaginary seawall slope that considers both the foreshore and structure slopes. While physically justified, the formulae first require the user to accurately estimate a characteristic wave run-up value before estimating wave overtopping. Furthermore, the method used to determine the imaginary slope is highly sensitive to the estimated water depth at the onset of wave breaking—which can vary depending on the wave transformation method or model applied.

More recently (Lashley et al., 2021b), derived a set of empirical formulae for very shallow foreshores that use deep-water wave conditions to directly predict the mean overtopping discharge at smooth, uniform slopes and vertical structures. Similar to the early wave overtopping design diagrams of Goda et al. (1975), these formulae account for the nonlinear effects of wave breaking using two terms that describe the foreshore: $h_{toe}/H_{m0,deep}$ and the foreshore slope angle (m). These two parameters have been successfully shown to determine the magnitude of several nearshore parameters for structures with shallow foreshores, including: the increase in mean water level referred to as wave setup (Goda, 2000; Gourlay, 1996; Lashley et al., 2021b); the significant wave height: H_{m0} (Lashley et al., 2021b) and $H_{1/3}$ (Goda, 2000); the spectral wave period ($T_{m-1,0}$) (Hofland et al., 2017); and the height of infragravity waves, also referred to as "surfbeat" or "dynamic setup" (Goda, 2000; Lashley et al., 2020a).

The overtopping formulae developed by Lashley et al. (2021b) proved accurate when applied to the physical (scale) model tests used to derived them—with simple uniformly sloping foreshore and structure slopes. However, like many other empirical overtopping models, the formulae have yet to be validated in the field. Field validation of empirical methods is necessary because field conditions (e.g., structure geometry and foreshore bathymetry) often vary from the controlled laboratory conditions used to derive them. This process not only quantifies the potential differences but also presents an opportunity to adjust or extend the methods to better bridge the gap between the laboratory and reality. Despite their importance, field measurements of wave overtopping are very rare due to the following reasons: i) storm conditions that result in significant wave overtopping are very infrequent (with very low annual probabilities of occurrence); and ii) deployment of the collection tanks typically used to measure wave overtopping in the field is very costly due to their size and weight (Briganti et al., 2005; Pullen et al., 2012; Troch et al., 2004).

Acknowledging these challenges, Van der Meer et al. (2019) proposed a unique approach at Eemshaven (the Netherlands) where overtopping tanks were cut and placed into the dike, essentially lowering the effective crest level and allowing for overtopping measurements under yearly storm conditions over the course of 12 years. However, such a method that requires the direct cutting and modification of the structure may not be easily implemented at other locations. On the other hand, Oosterlo et al. (2021) proposed a more flexible approach, which makes use of two laser scanners (LIDARs), attached to a relocatable pole, to measure the front velocity and layer thickness of wave run-up. These measurements may then be used to calculate a "virtual" overtopping discharge by assuming a hypothetical crest level and a relation between the maximum run-up volume and the actual overtopping volume. While this approach is readily adaptable, the reliability of the approach is subject to weather conditions (affecting the reflected signal intensity), blockage (e.g., a person standing in front of the beam), and the assumptions made.

More recently, two novel methods have been applied at Crosby (Northwest England), where the 900-m long coastal defence experiences overtopping every spring tide with an onshore wind. The first makes use of crowd-sourcing (or citizen science) methods, where residents of Crosby indicate—with photos via social media—when and where wave overtopping occurs (Brown et al., 2021). This approach is similar to the use of "YouTube" videos by Sandoval and Bruce (2018) to identify and analyse wave overtopping events. It recognises the utility of social media for the rapid collection (and dissemination) of information during extreme and more frequent nuisance overtopping events—providing a valuable data source for the qualitative validation of flood models (Khan et al., 2022; Smith et al., 2017). The second and more innovative approach at Crosby uses low-cost materials and an easily relocatable frame that supports a system of capacitance wires, termed "WireWall" (Section 2.2.1). The system, which has been validated using an extensive set of tests in a 2D wave basin, is capable of accurately measuring both individual wave overtopping volumes and mean overtopping discharge (Yelland et al., 2022).

The coastal defence at Crosby includes a stepped revetment and recurve wall, fronted by a shallow sandy beach with a ridge system on the upper beach approximately 50 m before the structure. At that site, wave overtopping alerts and warnings are issued by the Environment Agency (EA) when the estimated mean overtopping discharge—calculated using 15-min averaged now-cast offshore wave data—exceeds 2 l/s/m and 25 l/s/m, respectively. However, alerts were rarely issued for notable overtopping events that were reported via social media during the 2013 to 2018 period (Brown et al., 2020b). This suggests that the approach used by the EA to predict wave overtopping, based on SWAN and an older version of the EurOtop (2007) manual using a past beach level (that is higher than that seen during the relevant period), may not be suitable for the shallower present-day conditions at Crosby.

Recently, SWAN-Bayonet GPE (Pullen et al., 2018)—a meta-modelling approach comparable to a neural network—has been applied to estimate wave overtopping at Crosby (Brown et al., 2020a). This approach is based on the latest EurOtop (2018) manual, which is considered the industry standard for wave overtopping globally. However, as the name suggests, this approach still requires that the practitioner first use SWAN to transform waves from offshore to the structure toe. While SWAN may perform well for conditions with $h_{toe}/H_{m0,deep} \geq 1$, it is expected to underestimate the wave height and period at the structure toe for shallower cases, as demonstrated in several modelling studies (Buckley et al., 2014; Lashley et al., 2020b; Salmon and Holthuijsen, 2015; van der Westhuysen, 2010).

In light of this, it is our primary aim here to use the data gathered using the above-mentioned novel techniques to assess the accuracy and viability of the deep-water-parameter-based approach proposed by Lashley et al. (2021b) (Equation (1) of this paper), as an alternative to SWAN-Bayonet GPE for very shallow conditions. Our secondary objective is to compare the overtopping discharge predicted using the newly validated formulae to those made using the older SWAN and EurOtop (2007) approach (which represents the current EA method) for the range of offshore wave and water level combinations when overtopping was reported by the community via social media. In this way, we aim to identify any potential limitations of the current EA method to help improve the coastal hazard early warning system at that location.

1.2. Outline

This paper is organized as follows: Section 2 describes the study site and the field data collected using the WireWall system and social media reports. Section 2 also details the deep-water-parameter-based approach (Lashley et al., 2021b), along with the SWAN Bayonet GPE (Pullen et al., 2018) and SWAN-EurOtop (2007) approaches, which are used here for benchmarking. In Section 3, the overtopping estimates are compared quantitatively to the WireWall field measurements and qualitatively to the photographic reports made via social media. The validity of the deep-water-parameter-based approach is discussed along with the likelihood of wave overtopping at Crosby for non-extreme offshore wave and water level combinations. Section 4 concludes the paper by addressing the overall research objectives, stating limitations and identifying areas for future work.

2. Methods

2.1. Study site

The study site is located at Crosby in the Northwest of England (Brown et al., 2020b) (Fig. 1), which is exposed to a tidal range of 10 m and deep-water significant wave heights ($H_{m0,deep}$) exceeding 3.4 m, during annual storms (as frequent as once every three months). The coastal defence includes a 1:2.5 sloping stepped revetment and a recurve wall with a crest height of approximately 6.4 m AOD (above ordnance datum) (Fig. 2). In front of the structure, a wide, gently sloping beach with a bar and trough system—also referred to as a ridge and runnel system—functions as a shallow foreshore by initiating wave breaking during storms (Fig. 3). Considering the difference between the maximum and minimum bed levels (Δz) recorded from September 1996 to January 2019 (a total of 32 profiles available from: https://coastalmonitoring.org), the lower beach ($x < -200$ m) experiences less variability ($\Delta z = 0.35$ m, on average) than the ridge system of the upper beach ($x > -200$ m with $\Delta z = 0.93$ m, on average). In addition to long-term variability, it is important to note that the beach profile can experience both erosion and deposition over the course of single storm. However, this short-term variability is not considered here, as no incremental profile measurements were taken during the events.

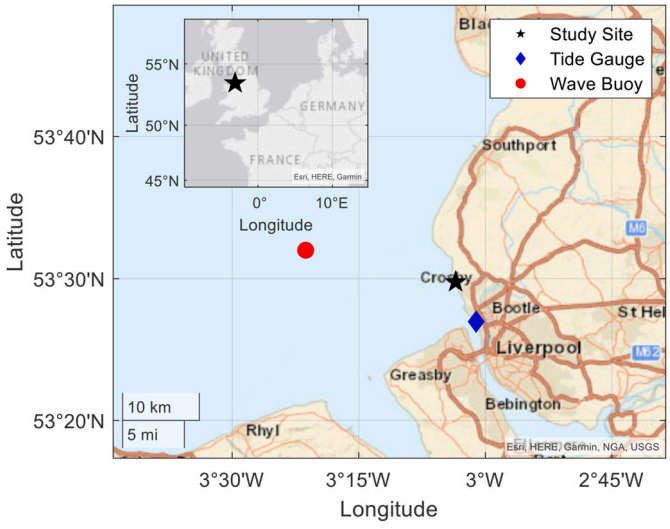

Fig. 1. Map of the study site showing the locations of the tide gauge and offshore wave buoy used in this study. Inset shows the location of the study site relative to the wider UK.

Fig. 2. Photo of the coastal defence at Crosby with foreshore exposed at low tide.

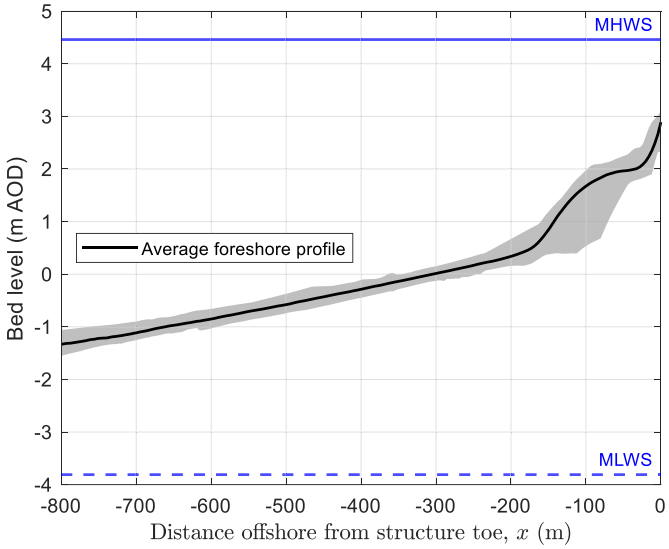

Fig. 3. The average foreshore profile recorded from September 1996 to January 2019, showing the bar-trough system (-200 m $< x < -30$ m), with bed level given in meters above ordnance datum (m AOD). The shaded area represents the maximum and minimum bed levels recorded during that period. Mean high water spring (MHWS) and mean low water spring (MLWS) levels are shown for reference.

2.2. Field observations

2.2.1. WireWall

The WireWall system (Brown et al., 2020b; Yelland et al., 2022) was developed to be a relatively low-cost tool in field measurements of wave overtopping to help optimize the design of coastal defences and early warning processes. The system incorporates a three-dimensional grid of vertical capacitance wires that record the length of the wires in contact with water, and the speed of the water passing through the grid (Fig. 4). In this way, the system can measure the volume and speed of individual waves as they overtop the structure.

WireWall was deployed during a few spring high tides at Hall Road Crosby in winter 2018–2019, where it recorded wave overtopping on January 25th, 2019 from 13:21 to 14:21. During this period, the average water depth at the structure toe (h_{toe}), $H_{m0,deep}$, offshore spectral wave period ($T_{m-10,deep}$), and directional spreading (σ) were 1.6 m, 1.7 m, 5.7 s

Fig. 4. WireWall system installed at Crosby as a wave overtops the structure.

and 19.7°, respectively (Fig. 5). The standard deviations associated with these values were: 0.12 m, 0.04 m, 0.06 s and 2.89°, respectively.

The water level data was obtained from the Gladstone Liverpool Dock tide gauge (Fig. 1 and available from: Tide Data), while the offshore wave data (in 24 m water depth) was obtained from the CEFAS database for Liverpool Bay WaveNet Site (Fig. 1 and available from: Wave Data). The above parameter values indicate a wind-sea wave climate and a very shallow condition at the structure toe: $h_{toe}/\ H_{m0,deep}$ varied from 0.91 to 1.04 (average of 0.94) during the 1-h period that overtopping occurred. A beach profile collected during low water on January 25th, 2019, was used to estimate the local water depth.

The wave-by-wave overtopping volume measurements obtained by the WireWall system were averaged over 15-min periods and converted to a 15-min discharge rate (q), which ranged from 3 to 10 l/s/m

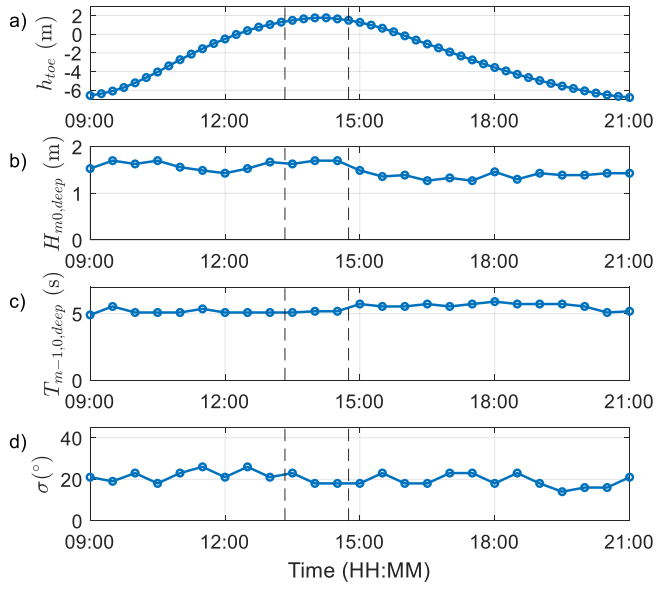

Fig. 5. Time series of: a) water depth relative to the structure toe; b) offshore significant wave height; c) offshore spectral wave period; and d) directional spreading, on January 25th, 2019, obtained from the Liverpool tide gauge and CEFAS WaveNet buoy at Liverpool. Dashed lines indicate the period when conditions were relatively constant and wave overtopping was measured.

(available from: WireWall Data (Brown et al., 2020a)). This 15-min period is consistent with the 15-min intervals used by the EA to now-cast hazard information. As the variation in forcing was minor during the hour when overtopping occurred—consistent with a single sea-state—the measurements were further averaged over that entire period to produce a 1-h averaged q of 4 l/s/m.

2.2.2. Social media reports

In December 2013, an open-access community Facebook page was established for Crosby with the title, "I'm at Crosby beach and the weather is …" (Facebook Page) and community members were able to report when wave overtopping of any magnitude occurred (Brown et al., 2021). Using the photographs from the page (Fig. 6) along with others supplied by local coastal managers/contractors (for the period January 2013 to December 2017) to identify the dates of overtopping events, the corresponding foreshore profiles (available from: https://coastalmonitoring.org), water levels and wave conditions were extracted from the national monitoring networks. The data was extracted at 15-min intervals for the 4-h periods centred over each high tide on the date reported. The resulting dataset included a total of 1 080 wave and water level combinations (over 41 days) that satisfied the shallow to emergent toe conditions ($-0.2 < h_{toe}/H_{m0,deep} \leq 1.5$), where Equation (1) is valid.

2.3. Deep-water-parameter-based wave overtopping

2.3.1. Main formulae

Here, we apply the deep-water-parameter-based formulae developed by Lashley et al. (2021b) to estimate q at smooth, sloping structures with shallow foreshores, including the effects of infragravity waves. The formulae, presented below, were derived using data from 389 physical (scale) model tests with varying wave, water level, foreshore slope angle and structure slope angle conditions (Table 1):

$$\frac{q}{\sqrt{g \cdot H_{m0,deep}^3}} = d \cdot \exp\left(-e \cdot \frac{R_c}{H_{m0,deep}} + f \cdot \frac{h_{toe}}{H_{m0,deep}} \right). \quad (1)$$

For very shallow cases (regime 1), with $0.5 \leq h_{toe}/H_{m0,deep} \leq 1$:

$$d_1 = 1.90 \cdot s_{om-1,0}^{1.15}; \quad (2)$$

Fig. 6. Example photo obtained from the Facebook page, posted by a community member on February 8th' 2016, showing significant wave overtopping at Crosby, UK (Brown et al., 2021).

Table 1
Valid range of parameters for application of Equations (1)–(7).

Parameter	Range
h_{toe} /$H_{m0,deep}$	−0.2 to 1.5
R_c /$H_{m0,deep}$	0.2 to 2.6
$s_{om-1,0}$	0.007 to 0.063
$\tan(m)$	1:250 to 1:10
$\tan(\alpha)$	1:7 to 1:2

$$e_1 = 7.40 \cdot \frac{s_{om-1,0}^{0.60}}{\tan(m)^{0.25} \cdot \tan(\alpha)^{0.60}}\ ; \tag{3}$$

and,

$$f_1 = 0.70 \cdot \frac{\tan(m)^{0.80}}{s_{om-1,0}^{0.80}}\ . \tag{4}$$

where R_c is the crest freeboard, $s_{om-1,0}$ is the wave steepness based on $H_{m0,deep}$ and the spectral wave period in deep water ($T_{m-1,0,deep}$), α is the structure slope angle and m is the foreshore slope angle (Fig. 7). For cases with highly irregular foreshores, m is taken as a single hypothetical slope (defined in Section 2.3.2).

For extremely shallow or emergent cases (regime 2), with $h_{toe}/H_{m0,deep} \leq 0.1$:

$$d_2 = 1.35 \cdot \tan(m)^{0.35} \cdot s_{om-1,0}^{0.85}; \tag{5}$$

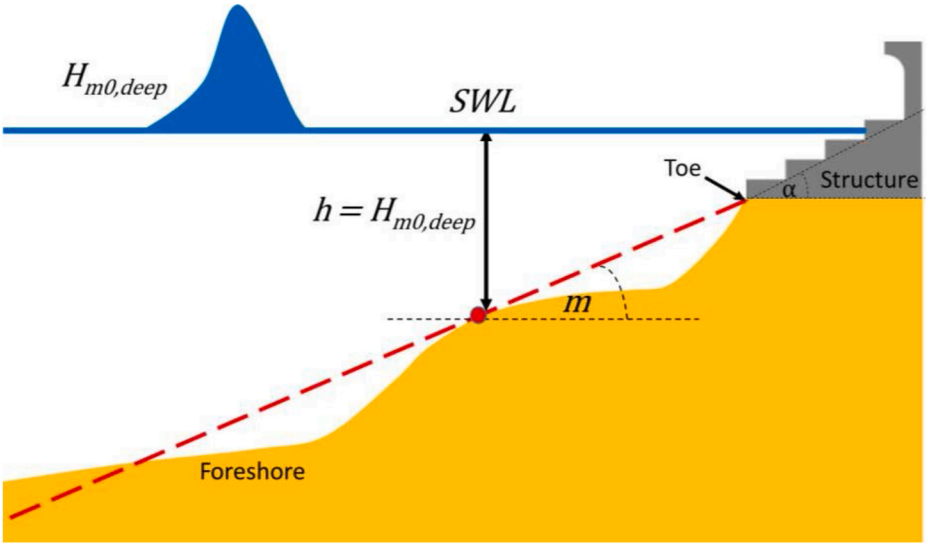

Fig. 7. Schematic representation of the foreshore and structure at Crosby (UK) showing the hypothetical foreshore slope angle (***m***) used in this study.

$$e_2 = 3.75 \cdot \frac{s_{om-1,0}^{0.70}}{\tan(m)^{0.70} \cdot \tan(\alpha)^{0.60}} \; ; \tag{6}$$

and,

$$f_2 = 0.20 \cdot \frac{s_{om-1,0}^{0.35}}{\tan(m)^{1.30}} \; . \tag{7}$$

with exponential interpolation between the two regimes ($0.1 > h_{toe} / H_{m0,deep} < 0.5$). While developed primarily of conditions where $h_{toe}/H_{m0,deep} \leq 1$, the maximum of Equation (1) (for $h_{toe}/H_{m0,deep} = 1$) may also be used to estimate q for less shallow conditions ($1 < h_{toe} / H_{m0,deep} < 1.5$). The reliability of Equations (1)–(7) is expressed in terms of a geometric standard deviation, $\sigma(\overline{x}_G) = 1.90$, where the 95% confidence intervals are given by $q \cdot \sigma(\overline{x}_G)^{(\pm 2)}$.

2.3.2. Hypothetical foreshore slope

Given the irregular nature of the foreshore at Crosby, it is important that the foreshore slope angle parameter (m) be accurately prescribed in Equations 1 to 7, 13 and 14—which were developed using physical and numerical tests with uniformly sloping foreshores. Here, m is defined simply as the (hypothetical) constant slope angle, extending from a depth, $h = H_{m0,deep}$ to the structure toe (Fig. 7).

While the use of hypothetical slopes with empirical methods is common, the approach used here differs largely from other methods that aim to define a single slope to represent both the foreshore and structure together (Altomare et al., 2016; Mase et al., 2013; Saville Jr, 1957). The characteristic depth ($h = H_{m0,deep}$) is considered the point where the foreshore begins to significantly affect the magnitude of nearshore/-shoreline parameters, such as: $H_{m0,toe}$, $T_{m-1,0,toe}$, wave setup and q (Hofland et al., 2017; Lashley et al., 2021b). This is also made evident by the Goda (2000) design diagrams for estimating the wave height ($H_{1/3}$) in the surf zone—where the relationship between the change in wave height ($H_{1/3} / H_0^{'}$) and relative water depth becomes linear when $h/ H_0^{'} \leq 1$, with $H_0^{'}$ considered to be the same as $H_{m0,deep}$.

In the above approach, m varies depending on the offshore wave height and local water depth conditions. As often done in practice, a maximum foreshore slope of 1:10 is considered (EurOtop, 2018). The appropriateness of this approach was assessed and verified using the XBeach Non-hydrostatic and SWAN numerical models by comparing the characteristics of wave propagation for: i) the irregular (real) foreshore and ii) the hypothetical foreshore slope, as defined here. The results of that analysis are presented and discussed in Appendix A.

2.4. Influence factors

As the above formulae were developed for simple structures with smooth slopes, the estimated overtopping discharge must be modified to account for the influence of the stepped revetment and parapet wall. These influence factors (γ) are typically obtained by comparing physical model tests for a structure with a particular feature (e.g. stepped revetment or recurve wall) to a reference case (usually a straight slope) (EurOtop, 2018). They are usually expressed as:

$$\gamma = \frac{\ln(q_{reference})}{\ln(q_{feature})} \; , \tag{8}$$

2.4.1. Influence of stepped revetment

The influence of the stepped revetment can be interpreted as an increased roughness or friction compared to a slope without any roughness elements or features. EurOtop (2018) recommends minimum and maximum friction factors (γ_f) of 0.75 and 0.9, respectively for roughness elements. The manual also notes that the influence varies depending on the water level, as elements below the still water line tend to have less influence. To account for this, a variable γ_f was used here. A value of 0.9 was applied for cases where the water level reached the top step and 0.75 was applied when the water levels were at the toe, with linear interpolation between these values for intermediate water levels. It should be noted that the Kerpen et al. (2019) approach, where γ_f is a function of α, step height and wave height at the toe, was also considered and yielded similar γ_f values (not shown) to the variable approach taken here.

2.4.2. Influence of recurve wall

Similarly, we adopted the EurOtop (2018) approach to account for the influence of the recurve wall (referred to as a "wall + bullnose" in the manual). The reduction factor (γ^*) is given by:

$$\gamma^* = \gamma_v \cdot \gamma_{bn} \cdot \gamma_{s0,bn}, \tag{9}$$

where,

$$\gamma_v = \cdot \exp\left(-0.56 \cdot \frac{h_{wall}}{R_c} \right), \tag{10}$$

$$\gamma_{bn} = 1.8 \cdot \left(1.53 \cdot 10^{-4} \cdot \varepsilon^2 - 1.53 \cdot 10^{-2} \cdot \varepsilon^2 + 1\right) \cdot \left(0.75 - 0.20 \cdot \frac{h_n}{h_{wall}}\right), \tag{11}$$

$$\gamma_{s0,bn} = 1.33 \cdot 10 \cdot s_{tm-1,0}, \tag{12}$$

where h_{wall} (= 0.97 m) is the height of the wall; h_n (= 0.47 m) is the thickness of the bullnose; ε is the bullnose angle (taken here as 45°) (Fig. 8); and $s_{tm-1,0}$ is the wave steepness calculated using the significant wave height at the toe ($H_{m0,toe}$) and the wave period at the structure toe ($T_{m-1,0,toe}$). The parameter validity range for Equations (9)–(12) are provided in Table 2.

Here, $H_{m0,toe}$ was estimated using the following empirical expression (Equation (13)), which accounts for the influence of wave setup and infragravity waves generated by waves breaking over shallow foreshores (Lashley et al., 2021b):

$$\frac{H_{m0,toe}}{H_{m0,deep}} = \left(0.35 \cdot \frac{\tan(m)^{0.10}}{s_{om-1,0}^{0.20}}\right) \cdot \frac{h_{toe}}{H_{m0,deep}} + \left(0.95 \cdot \tan(m)^{0.15} - 0.30\right) \tag{13}$$

which is considered valid for 1:1 000 $\leq \tan(m) \leq$ 1:10; $-0.14 \leq h_{toe} / H_{m0,deep} \leq 1$; and $0.006 \leq s_{om-1,0} \leq 0.06$. In a similar approach, $T_{m-1,0,toe}$ was estimated as follows (Lashley et al., 2021a):

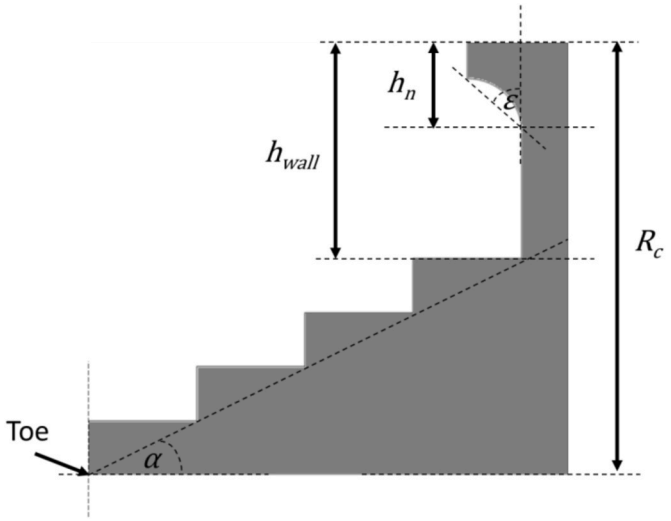

Fig. 8. Schematic representation of the structure at Crosby (UK) comprising a stepped revetment and recurve wall, highlighting key variables: structure slope angle ($\boldsymbol{\alpha}$), bullnose thickness ($\boldsymbol{h_n}$) and height of the recurve wall ($\boldsymbol{h_{wall}}$).

Table 2
Valid range of parameters for application of Equations (9)–(12).

Parameter	Range
h_n / h_{wall}	0.125 to 1
h_{wall} / R_c	0.11 to 0.90
ε	15°, 30°, 45° and 60°
R_c / $H_{m0,toe}$	>0.6
$s_{tm-1,0}$	0.01 to 0.05
$\tan(\alpha)$	1:3 to 1:2

$$\frac{T_{m-1,0,toe}}{T_{m-1,0,deep}} = \begin{cases} 1.59 \cdot \widetilde{H}_{IG}^{0.69} \cdot \cot(m)^{0.17} & \frac{h_{toe}}{H_{m0,deep}} \le 1 \\ 1 & \frac{h_{toe}}{H_{m0,deep}} > 1 \end{cases}, \quad (14)$$

where $\widetilde{H}_{IG}$ is the estimated ratio of the infragravity to sea-swell wave heights at the structure toe (Appendix B). Equation (14) is considered valid for 1:1 000 ≤ $\tan(m)$ ≤ 1:10. Note that an alternative method to estimate $T_{m-1,0,toe}$ by Hofland et al. (2017) could also be applied here and is expected to produce similar results.

Alternative approaches to account for the recurve wall, such as of those Owen and Steele (1993) and Coeveld et al. (2007), were also considered. However, the structure and forcing characteristics here were found to be outside their respective validity ranges.

2.5. Alternative overtopping methods for benchmarking

To benchmark to the performance of the deep-water-parameter-based approach (Section 2.3), two additional overtopping methods were considered for comparison:

i. SWAN-Bayonet GPE, a calculation tool based on the latest wave overtopping guidance (EurOtop, 2018); and
ii. SWAN-EurOtop (2007), which represents the method used by the EA to issue alerts and warnings for the period of January 2013 to December 2017. This approach is based on an older version of EurOtop (2007) manual.

2.5.1. SWAN-bayonet GPE

Bayonet GPE (Pullen et al., 2018) is a free empirical wave overtopping tool (available from: www.overtopping.co.uk). It uses the Gaussian process emulation (GPE) technique to essentially interpolate between the 13,500 known data points that underlie the EurOtop (2018) manual. The approach uses the phase-averaged wave model, SWAN (Booij et al., 1999) in 1D mode to transform offshore wave conditions to the structure toe. These nearshore parameters, along with those that describe the geometry of the structure, are then fed into Bayonet GPE to predict q.

SWAN-Bayonet GPE wave overtopping predictions (15-min averaged) were hindcasted for the January 25th, 2019 event at Crosby and published online (Brown et al., 2020a). Like with the deep-water-parameter-based formulae, the stepped revetment and recurve wall were considered using the influence factors outlined in Section 2.4.

2.5.2. SWAN-EurOtop (2007)

The EA's flood forecasting service uses a similar approach based on an older version of EurOtop (2007) manual, which is still considered the best practice for flood forecasting in England and Wales (Brown et al., 2020b). To represent the EA's hazard predictions for the period of January 2013 to December 2017, estimates of q were made using SWAN and the EurOtop (2007) empirical formulae, which follow:

$$\frac{q}{\sqrt{g \cdot H_{m0,toe}^3}} = \frac{0.067}{\sqrt{\tan(\alpha)}} \cdot \xi_{m-1,0} \cdot \exp\left(-4.75 \cdot \frac{R_c}{\xi_{m-1,0} \cdot H_{m0,toe}} \right), \quad (15)$$

$$\xi_{m-1,0} = \frac{\tan(\alpha)}{\sqrt{s_{tm-1,0}}}, \quad (16)$$

for $\xi_{m-1,0} < 5$, with a maximum of,

$$\frac{q}{\sqrt{g \cdot H_{m0,toe}^3}} = 0.2 \cdot \exp\left(-2.6 \cdot \frac{R_c}{H_{m0,toe}} \right). \quad (17)$$

The reliability of Equations (15) and (17) is described by taking the coefficients 4.75 and 2.6 as normally distributed stochastic parameters with means of 4.75 and 2.6 and standard deviations of 0.5 and 0.35, respectively (EurOtop, 2007).

For waves breaking over shallow foreshores, with $\xi_{m-1,0} > 7$, EurOtop (2007) recommends:

$$\frac{q}{\sqrt{g \cdot H_{m0,toe}^3}} = 10^c \cdot \exp\left(-\frac{R_c}{H_{m0,toe} \cdot (0.33 + 0.022 \cdot \xi_{m-1,0})} \right), \quad (18)$$

where the coefficient c has a mean value of −0.92 and a standard deviation of 0.24. For 5 < $\xi_{m-1,0}$ < 7, the user should use linear interpolation between Equation (15) or 17 and Equation (18). Note that for this SWAN-EurOtop (2007) approach, the $H_{m0,toe}$ and $T_{m-1,0,toe}$ parameters used in Equations (15)–(18) were obtained using SWAN. The stepped revetment and recurve wall were also considered here using the influence factors outlined in Section 2.4

3. Results and discussion

3.1. WireWall data averaged over the full overtopping duration (1 h)

We first assess the ability of the deep-water-parameter-based approach (Equations (1)–(7)) to predict q, averaged over the 1 h that wave overtopping occurred during the WireWall deployment on January 25th, 2019 (Yelland et al., 2022). Without including the overtopping reduction effects of the stepped revetment and recurve wall, q is initially overestimated by a factor of 10 (Fig. 9). However, when the influence factors are incorporated, the estimated q agrees well with the

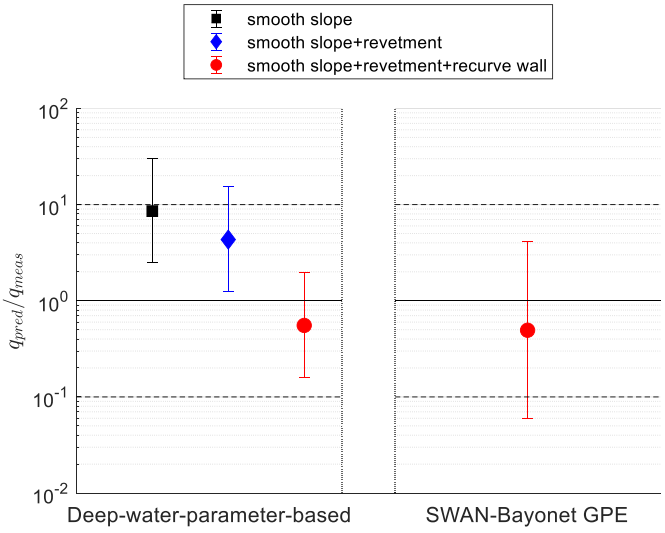

Fig. 9. Ratio of predicted to measured (WireWall) mean overtopping discharge (q_{pred}/q_{meas}) averaged over the 1 h that wave overtopping occurred on January 25th, 2019. Error bars represent the uncertainty (95% confidence intervals) for the overtopping predictions.

WireWall measurements—with the ratio of predicted to measured q (q_{pred}/q_{meas}) within a factor of 2. The performance of the deep-water-parameter-based approach was also on-par with the SWAN-Bayonet GPE approach (Fig. 9), which represents the industry standard (EurOtop, 2018).

As both approaches use the same influence factors to account for the stepped revetment and recurve wall, their comparison here is considered a fair assessment of how well q was estimated—i.e., even without influence factors. The main difference between the two approaches is how the effects of the foreshore are considered. In the deep-water-parameter-based approach, the foreshore is directly considered by the hypothetical slope angle (m) and relative water depth ($h_{toe}/H_{m0,deep}$). On the other hand, the SWAN-Bayonet GPE approach does not include m as an input parameter but assumes that the foreshore effects are accurately modelled by SWAN. For the conditions here, where only minor wave breaking takes place on the foreshore directly in front of the structure, the SWAN model performed well. However, for shallower conditions with heavy wave breaking over the foreshore, infragravity waves (also known as "surfbeat") are expected to play a significant role—resulting somewhat higher $H_{m0,toe}$ and significantly higher $T_{m-1,0,toe}$ values than those estimated by SWAN because the model does not directly resolve these long-wave motions. Therefore, the performance of the SWAN-Bayonet GPE approach is expected to decrease significantly with relative water depth unless the recently-developed SWAN SurfBeat version (Reniers and Zijlema, 2022) or empirical correction is applied (Lashley et al., 2021a).

3.2. Sensitivity of the deep-water-parameter-based approach to foreshore slope

As the deep-water-parameter-based approach uses the hypothetical foreshore slope angle (m) as one of its main input parameters, it is important to assess the sensitivity of the predicted q to potential errors or uncertainty in the determination of m. Fig. 10 shows that q increases with steeper foreshore slopes. Furthermore, for the same wave and water level forcing conditions, a change in $\tan(m)$ from 1:10 to 1:25 reduces the estimated q by one order of magnitude. This highlights the need to accurately define the representative foreshore slope for irregular bathymetries, particularly when assessing wave overtopping using a deep-water-parameter-based approach. Fig. 10 also demonstrates that the hypothetical foreshore slope ($\tan(m)$ = 1:10) obtained using the approach outlined in Section 2.3.2 and Appendix A, was a reasonable approximation of the actual foreshore; yielding a reasonably accurate estimate of q for the January 2019 event (Fig. 9).

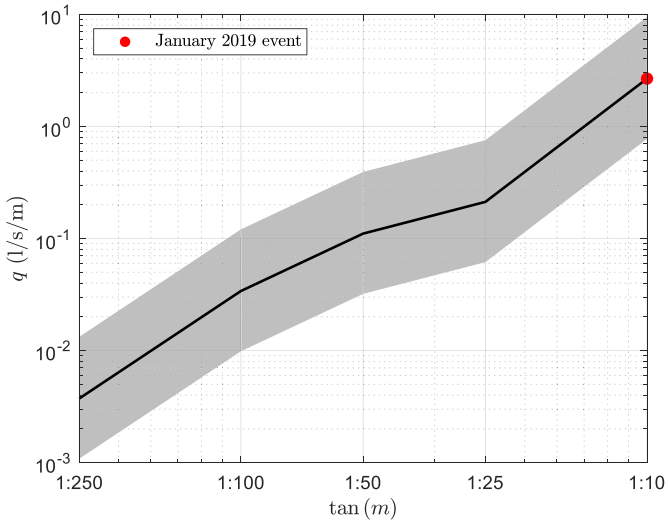

Fig. 10. Variation in deep-water-parameter-based q with $\tan(m)$ for $H_{m0,deep}$ = 1.7 m, $T_{m-10,deep}$ = 5.7s and h_{toe} = 1.6 m (conditions at Crosby on January 25th, 2019). Shaded area represents the uncertainty (95% confidence intervals) in Equation (1).

3.3. WireWall data averaged over 15-min intervals

Formulae for q, such as those applied here, are typically developed by dividing the total volume of overtopping water collected during physical model tests by the duration of the experiment. Given the random nature of an irregular wave climate, the selected duration needs to be sufficiently long (≥500 waves) such that the mean overtopping discharge obtained is statistically valid and comparable between tests (see Romano et al. (2015) for a detailed analysis on how the number of waves influences the overtopping discharge). Considering an average $T_{m-1,0,deep}$ of 5.2 s, the 1-h period of wave overtopping—where wave and water level conditions showed little variation at Crosby—corresponds to roughly 700 waves. This suggests that the deep-water-parameter-based approach can be reliably compared to the measured 1-h averaged q.

To assess the influence of storm duration and verify whether the approach is also suitable for very short-range (e.g., 15 min) forecasting, referred to as "nowcasting", we also compare the results from the deep-water-parameter-based approach to the WireWall measurements averaged over a 15-min period (Fig. 11a). As can be seen in Fig. 11a, the deep-water-parameter-based approach estimates q with reasonable accuracy (geometric mean and standard deviation of 0.46 and 1.9, respectively) despite the shorter (15-min) duration. It also performs marginally better than the SWAN-Bayonet GPE approach (geometric mean and standard deviation of 0.30 and 3.24, respectively). This is likely due to the SWAN model slightly underestimating the wave height and period at the toe of the structure at lower relative water depths (see Appendix A, for example) due to its exclusion of infragravity wave dynamics. This results in a minor underestimation of q (Fig. 11a), when the water level is lower (Fig. 11b).

It should be noted that neither the deep-water-parameter-based formulae nor the SWAN-Bayonet GPE approach were able to capture

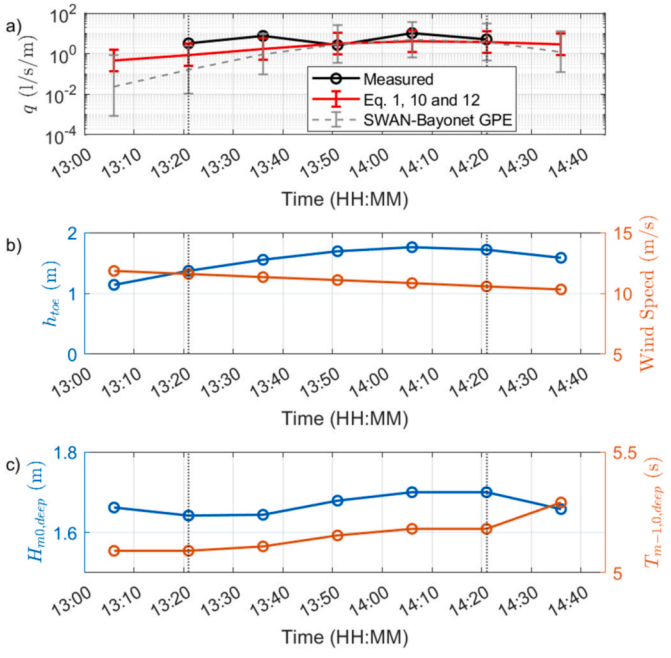

Fig. 11. a) Measured and predicted q at 15-min intervals on January 25th, 2019, showing b) the water depth at the structure toe (h_{toe}) and wind speed; and c) offshore significant wave height ($H_{m0,deep}$) and spectral wave period ($T_{m-1,0,deep}$). Note that all observations and SWAN-Bayonet predictions are resampled to the 15-min intervals that match the WireWall data. Dotted lines indicate the 1-h period when wave overtopping occurred.

the drop in measured q at time 13:51 (Fig. 11a). However, as this decrease does not coincide with a change in forcing—i.e. h_{toe} (Fig. 11b), $H_{m0,deep}$ or $T_{m-1,0,deep}$ (Fig. 11c)—we attribute this to the random nature of irregular waves. As wind is known to notably affect low overtopping volumes, a further check was made to determine whether a change in wind speed or direction explained the observed decrease in q using wind data from the local meteorological station (Brown et al., 2020b). However, wind speed only decreased slightly over the 1-h duration (Fig. 11b) while wind direction remained constant.

While the predictions compared well to the 15-min averaged observations, both the deep-water-parameter-based approach and SWAN-Bayonet GPE both estimated some wave overtopping for conditions at times 13:06 and 14:36, but no overtopping was recorded at the WireWall (Fig. 11a). This discrepancy is attributed to the shorter (15-min) duration where no waves overtopped the structure, while both prediction methods assume a duration ≥500 waves—where the opportunity for some waves to overtop the structure is greater. The takeaway here is that while the approach proved accurate when compared to observations here, empirical overtopping methods that assume a duration ≥500 waves may not match observations for shorter durations.

3.4. Social media reports

Next, we assess the ability of the deep-water-parameter-based approach to hindcast q for the 1 080 wave height and water level conditions on the days when wave overtopping was reported by the Crosby community, between January 2013 and December 2017 (Fig. 12a). Estimates were also made using the SWAN-EurOtop (2007) (Fig. 12b), which represents the method used by the EA to nowcast hazard information during the same period.

Given the logarithmic nature of the overtopping formulae, it is necessary to define a threshold below which the calculated overtopping discharge is considered zero. Using a threshold of 0.03 l/s/m for a non-zero overtopping discharge prediction (EurOtop, 2018), the deep-water-parameter-based approach estimated $q > 0.03$ l/s/m for 35 of the 41 days (85%) when wave overtopping was recorded via photographs. The exceptions occurred on days when the water levels (<3.6 m AOD) and offshore wave heights ($H_{m0,deep} \leq 0.9$ m) were particularly low (Fig. 12a). On the other hand, the SWAN-EurOtop (2007) approach estimated non-zero wave overtopping ($q > 0.03$ l/s/m) on only 30 of the 41 days (73%) reported. This is because the method only estimates non-zero overtopping discharges when the water level >4.0 m AOD and $H_{m0,deep} > 3.5$ m (Fig. 12b).

The validity of the deep-water-parameter-based approach at Crosby, compared to SWAN-EurOtop (2007), is verified here by two notable features of Fig. 12. First, the variation in the deep-water-parameter-based q with water level and $H_{m0,deep}$ matches well (in terms of magnitude) with the WireWall measurements made during the January 2019 event (Fig. 12a). This is however not the case for the SWAN-EurOtop (2007) estimates, which suggest one order of magnitude lower discharges for the same water level and $H_{m0,deep}$ conditions (Fig. 12b). Second, for the event reported via Facebook on February 8th, 2016, showing significant wave overtopping (Fig. 6), the deep-water-parameter-based approach estimated 10 l/s/m ≤ q ≤ 33 l/s/m (Fig. 12a), indicating that a hazard warning should have been issued (since $q > 25$ l/s/m). However, a warning would not have been issued for the event using the SWAN-EurOtop (2007) approach, where 2 l/s/m ≤ q ≤ 16 l/s/m (Fig. 12b)—despite the danger to pedestrians, evidenced by Fig. 6.

The lower estimates of q obtained using the SWAN-EurOtop (2007) approach are mainly due to the underestimation of $T_{m-1,0,toe}$ by SWAN (Appendix A), which is known to significantly affect the predicted overtopping discharge. This was demonstrated by Lashley et al. (2020b) who found that correcting the $T_{m-1,0,toe}$ calculated by SWAN using the Hofland et al. (2017) empirical formula, as recommended by EurOtop (2018), increased the estimated q by a factor of 10.

What is also noteworthy about Fig. 12a, is that q in excess of 10 l/s/m regularly occurs at Crosby when the water depth and offshore wave heights exceed 4.5 m AOD and 1.5 m, respectively. These conditions correspond to non-extreme (yearly) events and highlight the immediate need to improve hazard warning services at Crosby.

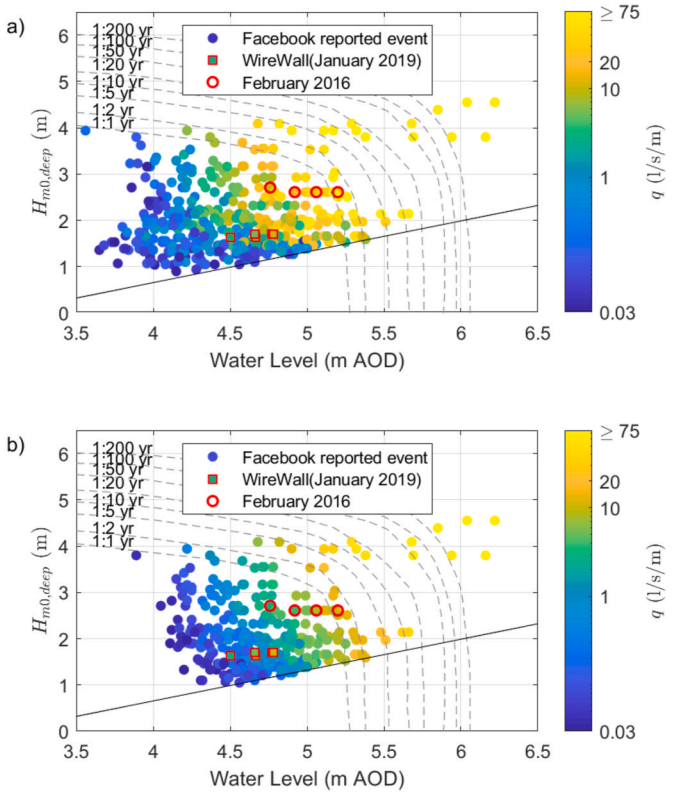

Fig. 12. Predicted mean overtopping discharge for the wave heights ($H_{m0,deep}$) and water levels corresponding to photographic records at Crosby from 2013 to 2018, using: a) the deep-water-parameter-based approach; and b) SWAN-EurOtop (2007); where the solid line corresponds to $h_{toe}/H_{m0,deep} = 1.5$. Joint probability curves (dashed lines) are provided for reference (Halcrow Group Limited, 2011). The measured 15-min averaged discharges for the January 2019 event are also provided for reference.

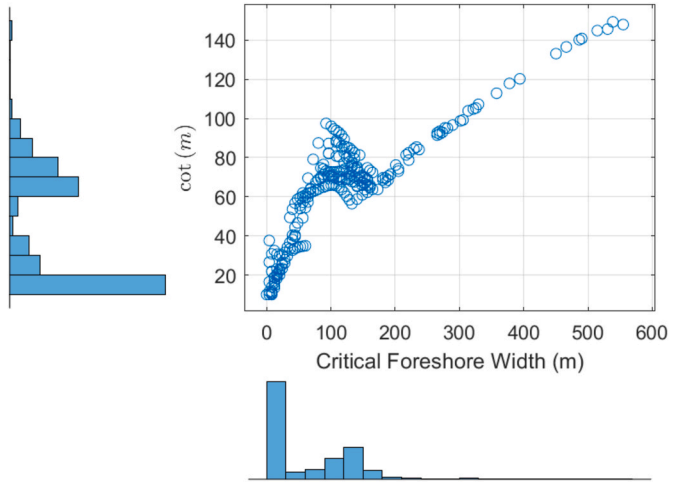

Fig. 13. Scatter plot with histogram of the critical foreshore width (x-axis) used to determine the hypothetical foreshore slope, $\mathbf{cot}(m)$ (y-axis) and predict q using the deep-water-parameter-based approach, for the 1 080 wave and water level conditions reported.

3.5. Critical foreshore width for wave overtopping at crosby

For the 1 080 wave and water level conditions reported via social media and their corresponding foreshore profiles, the offshore distance (critical foreshore width) used to determine the hypothetical foreshore slope angle (m) varied from immediately in front of the structure to over 550 m (Fig. 13). However, the distribution of this critical foreshore width suggests that the 200 m in front of the structure mostly influences wave overtopping at Crosby, with the first 30 m being the most critical—with $\tan(m) = 1{:}10$ (or $\cot(m) = 10$). This finding supports the conclusion of Brown et al. (2021) who found that the height of the beach within about 10 m of the structure toe had a strong influence on wave overtopping for any given wave and water level conditions. As the first 200 m in front of the structure is also the most dynamic (Fig. 3), coastal managers at Crosby can focus their surveying efforts on this limited beach area and still provide valuable information for flood risk assessments and forecasting.

4. Conclusions

Given high cost and high return periods for major storms, field measurements of wave overtopping are very limited. As a result, many empirical overtopping formulae are developed and validated using physical model tests and numerical simulations—without actual verification in the field. Moreover, many of the widely used overtopping formulae require wave parameters at the toe of the structure as input. For shallow foreshores where the nonlinear effects of wave breaking can dominate, this often requires that computationally demanding numerical models, and persons skilled in their application, be used to transform offshore waves to the structure toe.

In the present study, we validated a set of formulae for wave overtopping discharge (q) based on easily obtainable deep-water wave parameters. The validation was carried out using data gathered for the coastal defence (stepped revetment and recurve wall) and shallow foreshore at Crosby, UK. First, the formulae were compared quantitatively with wave overtopping measurements obtained using the WireWall system of capacitance wires in January 2019. Next, the deep-water-parameter-based approach was compared qualitatively to photographic records of wave overtopping obtained via community photos (from January 2013 to December 2017). For the WireWall data, the predicted q was within a factor of 2 of the measurements averaged over the full 1-h period when wave overtopping was measured and conditions were relatively constant, and within a factor of 4 of those averaged over 15 min. This suggests that the approach is appropriate for design and assessments—using the total duration of the event—and forecasting the time-varying hazard (at 15-min intervals) for operational hazard response management at Crosby.

Additionally, the hindcasts made for the events reported via Facebook corroborated the community reports, which indicated that overtopping discharges—under typical winter conditions—can exceed 10 l/s/m and pose a serious hazard to pedestrians. This finding, also reported by Brown et al. (2021), highlights the pressing need to improve the hazard forecasting and nowcast services at Crosby.

While the deep-water-parameter-based approach proved to be accurate here, it is still subject to certain limitations. For instance, the results highlighted the need to correctly define the representative foreshore slope angle (m), which is used as input to the formulae. The hypothetical foreshore slope method proposed here—where m is defined as a constant slope angle extending from a depth, $h = H_{m0,deep}$ to the structure toe—produced good results and may prove useful to practitioners who seek to parameterize surf zone processes (e.g. using the methods of Stockdon et al. (2006)) or make use of the well-known surf-similarity parameter (or "Iribarren number") (Battjes, 1974; Iribarren, 1949) in the field. However, it is recommended that the hypothetical foreshore slope method be further verified with physical model tests of different foreshore geometries (e.g., concave versus convex bottom profiles). Likewise, as our study was limited to the conditions at Crosby (UK), it is also recommended that the accuracy of the overall deep-water-parameter-based approach to estimate q be verified at field sites with different hydrodynamic and geomorphological features, such as those with wider, milder foreshore slopes or those with larger offshore waves.

CRediT authorship contribution statement

Christopher H. Lashley: Conceptualization, Methodology, Validation, Formal analysis, Writing – original draft, Visualization. **Jennifer M. Brown:** Conceptualization, Methodology, Investigation, Resources, Data curation, Writing – review & editing. **Margaret J. Yelland:** Conceptualization, Methodology, Investigation, Resources, Writing – review & editing, Supervision, Project administration, Funding acquisition. **Jentsje W. van der Meer:** Conceptualization, Methodology, Writing – review & editing, Supervision. **Tim Pullen:** Investigation, Software, Data curation.

Declaration of competing interest

The authors declare that they have no known competing financial interests or personal relationships that could have appeared to influence the work reported in this paper.

Data availability

Data will be made available on request.

Acknowledgements

The authors acknowledge CEFAS and BODC for making the national monitoring data available. Finally, we acknowledge NERC innovation funding for the WireWall project (NE/R014019/1), which enabled the development of the first capacitance-based wave overtopping measurement system and its initial trials at Crosby. A. Martin (Sefton Council) is thanked for sharing his wave overtopping photos at Crosby.

Appendix A. Hypothetical Foreshore Slope Definition

For use with the deep-water-parameter-based formulae, m is defined here as the hypothetical constant slope angle from a depth, $h = H_{m0,deep}$ to the structure toe (Fig. 7). To verify the appropriateness of this approach, XBeach Non-hydrostatic (Smit et al., 2010) is used to simulate the change in wave height (H_{m0}) and spectral wave period ($T_{m-1,0}$) from offshore to the structure toe, for: i) the irregular (actual) bathymetry at Crosby measured in January 2019; and ii) the hypothetical foreshore slope angle (m). Note that the structure was replaced by a horizontal bed ($x > 0$ m in Figure A. 1 to Figure A. 3) in the numerical simulations to remove the influence of wave reflection. For the irregular bathymetry, the change in H_{m0} and $T_{m-1,0}$ is also estimated using SWAN (The SWAN Team, 2021) for comparison.

Both XBeach and SWAN are considered standard tools for wave propagation. The models are used here with default parameter values, with the following exceptions:

- For XBeach Non-hydrostatic (version XBeach X), the maximum breaking wave steepness parameter, $\lambda = 0.8$ following Lashley et al. (2020b) who found that λ varied from 0.7 to 0.9 for shallow foreshores under very mild and very steep wave conditions, respectively. A Manning's roughness coefficient ($n = 0.012$ s/m$^{1/3}$) is used to represent a smooth bottom. A constant cross-shore grid spacing ($\Delta x = 0.5$ m), which corresponds to > 100 grid cells per deep-water wavelength, was applied. The model was forced with JONSWAP wave spectra (spectra with a peak enhancement factor of 3.3) at its boundary.
- For SWAN (version 41.31), friction is specified using a Nikuradse geometrical roughness of 0.3×10^{-3} m (smooth bottom), in line with the Lashley et al. (2020b) benchmarking study for shallow foreshores. Consistent with the XBeach setup, a constant $x = 0.5$ m was applied, and the model was forced with JONSWAP wave spectra (spectra with a peak enhancement factor of 3.3) at its boundary. It should be noted that a coarser grid could have been used without loss of accuracy.

Figure A. 1 to Figure A. 3 show that H_{m0} begins to decrease on the foreshore slope due to wave breaking, where larger waves (with higher $H_{m0,deep}$ values) break further offshore. In the surf zone ($h \leq H_{m0,deep}$), wave breaking is dominant, and the waves are now considered depth-limited—where H_{m0} is directly dependent on the water depth and, hence, the foreshore profile. On the other hand, $T_{m-1,0}$ increases from offshore to the structure toe (Figure A. 1 to Figure A. 3) due to the reduction in wave energy at high frequencies and the growth of energy at low (infragravity) frequencies during wave breaking.

Considering the XBeach simulations for the conditions observed on January 25th, 2019, with $H_{m0,deep} = 1.7$ m, $h_{toe} = 1.6$ m (Figure A. 1), the modelled change in H_{m0} and $T_{m-1,0}$ for the irregular bathymetry is similar to that of a constant hypothetical foreshore slope angle (m) of 1:10. Simulations for both the irregular profile and $\tan(m) = 1{:}10$ show little difference between $H_{m0,deep}$ and $H_{m0,toe}$, as only minor wave breaking occurs directly in front of the structure toe (Figure A. 1a). The modelled change in $T_{m-1,0}$ show similar agreement between the two XBeach simulations; though the simulation with $\tan(m) = 1{:}10$ tends to underestimate the growth of $T_{m-1,0}$ as waves shoal over the irregular profile offshore ($x < -20$ m), resulting in a minor underestimation of $T_{m-1,0,toe}$ (Figure A. 1b).

When $H_{m0,deep}$ is increased to 2.7 m (while maintaining the same wave steepness), wave breaking initiates further offshore, with $h = H_{m0,deep}$ occurring ~60 m from the structure toe (Figure A. 2). Under these conditions, the characteristics of wave breaking are more comparable to those of a constant 1:60 foreshore slope. In like manner, for $H_{m0,deep} = 4.0$ m, the $\tan(m)$ that produces a similar reduction in H_{m0} (Figure A. 3a) and growth in $T_{m-1,0}$ (Figure A. 3b) to the irregular bathymetry becomes 1:75—with $h = H_{m0,deep}$ occurring ~170 m offshore (Figure A. 3).

It should be noted that the differences observed between the irregular bathymetry and constant slope simulations at x > −40 m for higher $H_{m0,deep}$ values (Figure A. 2a and Figure A. 3a) are due to the presence of the offshore trough (in the irregular profile), which greatly reduces wave breaking as the water depth becomes deeper. This process is not captured by the constant uniform slope. However, despite this minor disagreement, the $H_{m0,toe}$ and $T_{m-1,0,toe}$ values obtained using the constant slope were still within 20% of those obtained using the irregular bathymetry and are therefore considered acceptable.

Compared to XBeach, SWAN predicts a much earlier onset of wave breaking, resulting in much lower estimates of H_{m0} at the location where $h = H_{m0,deep}$ (Figure A. 1a, Figure A. 2a and Figure A. 3a). This discrepancy increases as $H_{m0,deep}$ increases, with SWAN predicting ~1 m lower wave heights than XBeach for the simulations with $H_{m0,deep} = 4.0$ m (Figure A. 3a). Despite these major differences offshore, both XBeach and SWAN tend to converge at the structure toe for lower $h_{toe}/H_{m0,deep}$ values (Figure A. 2a and Figure A. 3a). This is attributed to the depth-limited conditions immediately in front of the structure.

Additionally, SWAN does not capture the growth in $T_{m-1,0}$ from offshore to the structure toe (Figure A. 1b, Figure A. 2b and Figure A. 3b). This increase, which grows rapidly as $h_{toe}/H_{m0,deep}$ decreases (Figure A. 2b and Figure A. 3b), is due to the growth of long-period (infragravity) waves as the higher frequency (sea and swell waves) shoal and break over the foreshore (Longuet-Higgins and Stewart, 2006; Symonds et al., 1982). As this process is not resolved in SWAN, it consistently predicts almost no change in $T_{m-1,0}$. Equation (14) also shows no increase in $T_{m-1,0}$ for $h_{toe}/ H_{m0,deep} = 0.9$ (Figure A. 1b) but does capture the change for $h_{toe}/H_{m0,deep} = 0.4$—where the ratio of the spectral wave period at the toe to offshore, $T_{m-1,0,toe}/T_{m-1,0,deep} \approx 2.5$ (Figure A. 3b).

The overall trends observed in Figure A. 1 to Figure A. 3 highlight the dependence of the representative foreshore slope on the relative water depth ($h/H_{m0,deep}$) for highly irregular bathymetries. It also demonstrates that the approach taken here to define m may be considered reasonable. This is further supported by Equation (13): where the estimates of $H_{m0,toe}$ obtained using m compare well (within 15%) to those modelled by XBeach using the irregular bathymetry (Figure A. 1 to Figure A. 3); and Equation (14): where the estimates of $T_{m-1,0,toe}$ are within 20% of those modelled by XBeach (Figure A. 1 to Figure A. 3).

As no nearshore measurements were available for comparison, the above model results are considered conceptual and used here to: i) rationalise the approach taken to define m; and ii) compare the performance of Equations (13) and (14) in estimating wave conditions at the toe with the much more computationally demanding numerical modelling approaches. No further discussion on the accuracy of the predictions is dealt with here. It should also be acknowledged that it is more accurate to simulate the effects of an irregular bathymetry using XBeach Non-hydrostatic (or similar phase-resolving numerical model) compared to empirical estimates. However, the hypothetical foreshore slope—developed for use with the deep-water-parameter-based formulae—may be considered a practical and reasonably accurate alternative.

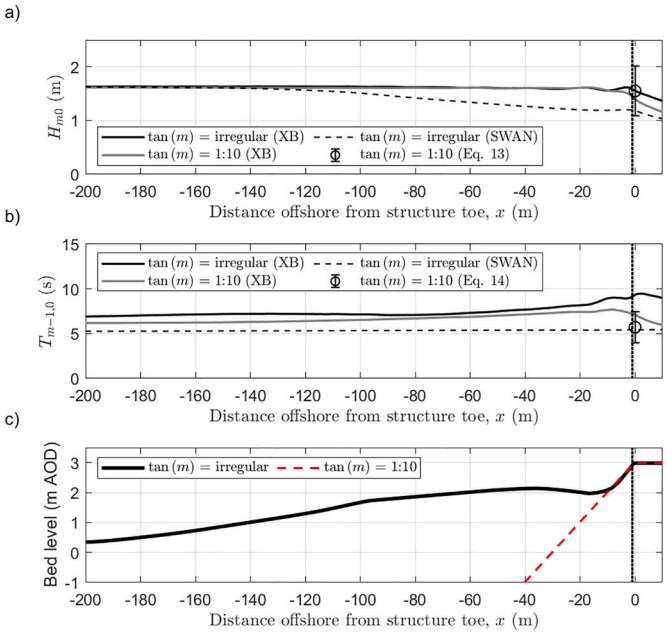

Figure A1. Modelled change in a) H_{m0} and b) $T_{m-1,0}$, from offshore to the structure toe using XBeach Nonhydrostatic and SWAN for $h_{toe} = 1.6$ m and $H_{m0,deep} = 1.7$ m ($h_{toe}/H_{m0,deep} = 0.9$); with c) the bed levels for the irregular bathymetry at Crosby and constant hypothetical foreshore slopes. Dotted vertical lines indicate $h = H_{m0,deep}$. Empirical estimates of $H_{m0,toe}$ (Equation (13)) and $T_{m-1,0,toe}$ (Equation (14)) are also provided with error bars (± 2 standard deviations). .

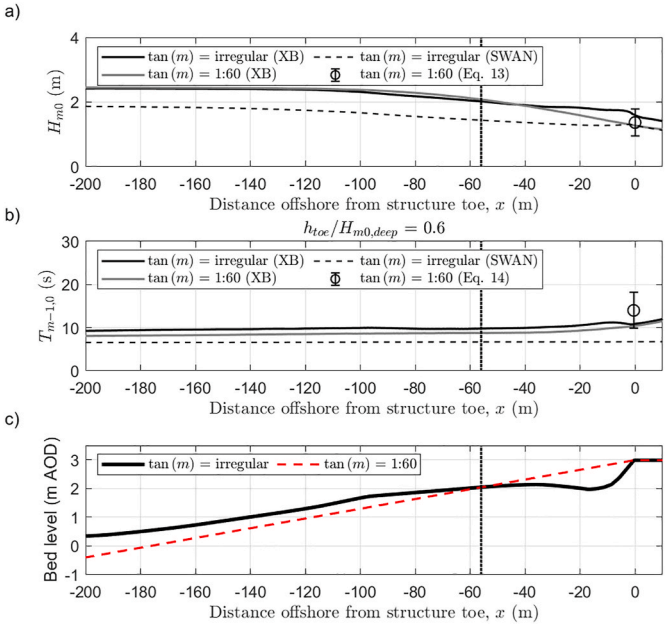

Figure A2. Modelled change in a) H_{m0} and b) $T_{m-1,0}$, from offshore to the structure toe using XBeach Nonhydrostatic and SWAN for $h_{toe} = 1.6$ m and $H_{m0,deep} = 2.7$ m ($h_{toe}/H_{m0,deep} = 0.6$); with c) the bed levels for the irregular bathymetry at Crosby and constant hypothetical foreshore slopes. Dotted vertical lines indicate $h = H_{m0,deep}$. Empirical estimates of $H_{m0,toe}$ (Equation (13)) and $T_{m-1,0,toe}$ (Equation (14)) are also provided with error bars (± 2 standard deviations).

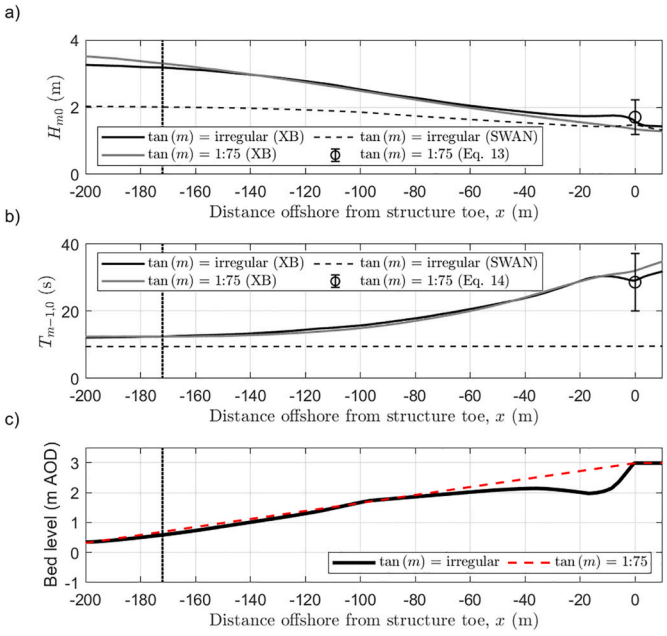

Figure A3. Modelled change in a) H_{m0} and b) $T_{m-1,0}$, from offshore to the structure toe using XBeach Nonhydrostatic and SWAN for $h_{toe} = 1.6$ m and $H_{m0,deep} = 4.0$ m ($h_{toe}/H_{m0,deep} = 0.4$); with c) the bed levels for the irregular bathymetry at Crosby and constant hypothetical foreshore slopes. Dotted vertical lines indicate $h = H_{m0,deep}$. Empirical estimates of $H_{m0,toe}$ (Equation (13)) and $T_{m-1,0,toe}$ (Equation (14)) are also provided with error bars (± 2 standard deviations).

Appendix B. Relative Magnitude of Infragravity Waves

The relative magnitude or significance of infragravity waves at the toe of a structure ($\widetilde{H}_{IG}$) may be expressed as (Lashley et al., 2020a):

$$\widetilde{H}_{IG} = 0.36 \cdot H_{m0,deep}^{0.5} \bullet \overline{\gamma}_{\sigma} \bullet \overline{\gamma}_{h} \bullet \overline{\gamma}_{fs}, \tag{B.1}$$

$$\overline{\gamma}_{\sigma} = 1 - 0.01 \bullet \sigma\ , \tag{B.2}$$

$$\overline{\gamma}_{h} = 1.04 \bullet \exp(-1.4 \bullet h_{toe}) + 0.9 \bullet \exp(-0.19 \bullet h_{toe}), \tag{B.3}$$

$$\overline{\gamma}_{fs} = \begin{cases} 1.56 - 3.09 \cdot \cot(m)^{-0.44} & \cot(m) \le 100 \\ 0.51 \cdot \cot(m)^{0.18} & \cot(m) > 100, h_{toe}/H_{m0,deep} \ge 0.2 \\ 1.62 \cdot \cot(m)^{-0.08} & \cot(m) > 100, h_{toe}/H_{m0,deep} < 0.2\ , \end{cases} \tag{B.4}$$

References

Altomare, C., Suzuki, T., Chen, X., Verwaest, T., Kortenhaus, A., 2016. Wave overtopping of sea dikes with very shallow foreshores. Coast. Eng. 116, 236–257.

Battjes, J.A., 1974. Surf Similarity, Delft, pp. 466–480.

Booij, N., Ris, R.C., Holthuijsen, L.H., 1999. A third-generation wave model for coastal regions: 1. Model description and validation. J. Geophys. Res.: Oceans 104 (C4), 7649–7666.

Briganti, R., Bellotti, G., Franco, L., De Rouck, J., Geeraerts, J., 2005. Field measurements of wave overtopping at the rubble mound breakwater of rome–ostia yacht harbour. Coast. Eng. 52 (12), 1155–1174.

Brown, J., Yelland, M., Pascal, R., Jones, D., Balfour, C., Hargreaves, G., Martin, B., Cardwell, C., Pinnell, R., Bell, P., 2020a. Key Wirewall Project Data Generated during the Field Deployment at Hall Road Crosby (North of Liverpool UK). https://doi.org/10.5285/acd939f0-38e7-57b0-e053-6c86abc0aa19 between October 2018 and March 2019.

Brown, J., Yelland, M., Pascal, R., Pullen, T., Cardwell, C., Jones, D., Pinnell, R., Silva, E., Balfour, C., Hargreaves, G., 2020b. Wirewall–a New Approach to Measuring Coastal Wave Hazard. http://nora.nerc.ac.uk/id/eprint/528538. National Oceanography Centre Research and Consultancy Report, 66.

Brown, J., Yelland, M., Pullen, T., Silva, E., Martin, A., Gold, I., Whittle, L., Wisse, P., 2021. Novel use of social media to assess and improve coastal flood forecasts and hazard alerts. Sci. Rep. 11 (1), 1–10.

Buckley, M., Lowe, R., Hansen, J., 2014. Evaluation of nearshore wave models in steep reef environments. Ocean Dynam. 64 (6), 847–862.

Coeveld, E., Busnelli, M., Van Gent, M., Wolters, G., 2007. Wave Overtopping of Rubble Mound Breakwaters with Crest Elements, Coastal Engineering 2006: (In 5 Volumes). World Scientific, pp. 4592–4604.

EurOtop, 2007. Eurotop—wave overtopping of sea defences and related structures. In: Pullen, T., et al. (Eds.), Assessment Manual. August. ISBN, pp. 978–3.

EurOtop, 2018. In: Van der Meer, J., et al. (Eds.), Manual on Wave Overtopping of Sea Defences and Related Structures. An Overtopping Manual Largely Based on European Research, but for Worldwide Application. Retrieved from www.overtopping-manual.com.

Goda, Y., 2000. Random Seas and Design of Maritime Structures, Advanced Series on Ocean Engineering. World Scientific Publishing, p. 464.

Goda, Y., Kishara, Y., Kamiyama, Y., 1975. Laboratory investigation on the overtopping rate of seawalls by irregular waves. Report of the Port Harbour Research Institute 14 (4), 3–44.

Gourlay, M.R., 1996. Wave set-up on coral reefs. 1. Set-up and wave-generated flow on an idealised two dimensional horizontal reef. Coast. Eng. 27 (3–4), 161–193.

Halcrow Group Limited, 2011. North West England and North Wales Smp2 - Supporting Studies, Joint Probability Studies - Extreme Wave Heights and Join-Sea Results.

Hofland, B., Chen, X., Altomare, C., Oosterlo, P., 2017. Prediction formula for the spectral wave period t m-1,0 on mildly sloping shallow foreshores. Coast. Eng. 123 (Suppl. C), 21–28.

Iribarren, C.R., 1949. Protection des ports. XVIIth International Naval Congress, Lisbon, Portugal, pp. 31–80, 1949.

Kerpen, N.B., Schoonees, T., Schlurmann, T., 2019. Wave overtopping of stepped revetments. Water 11 (5), 1035.

Khan, Q., Kalbus, E., Zaki, N., Mohamed, M.M., 2022. Utilization of social media in floods assessment using data mining techniques. PLoS One 17 (4), e0267079.

Lashley, C.H., Bricker, J.D., van der Meer, J., Altomare, C., Suzuki, T., 2020a. Relative magnitude of infragravity waves at coastal dikes with shallow foreshores: a prediction tool. J Waterw Port Coast 146 (5).

Lashley, C.H., Jonkman, S.N., Van der Meer, J., Bricker, J.D., Vuik, V., 2021a. The influence of infragravity waves on the safety of coastal defences: a case study of the

Dutch wadden sea. Natural Hazards and Earth System Sciences Discussions 2021, 1–40.
Lashley, C.H., Van Der Meer, J., Bricker, J., Altomare, C., Suzuki, T., Hirayama, K., 2021b. Formulating wave overtopping at vertical and sloping structures with shallow foreshores using deep-water wave characteristics. J. Waterw. Port, Coast. Ocean Eng. 147 (6), 04021036: 1-04021036: 13.
Lashley, C.H., Zanuttigh, B., Bricker, J.D., Van der Meer, J., Altomare, C., Suzuki, T., Roeber, V., Oosterlo, P., 2020b. Benchmarking of numerical models for wave overtopping at dikes with shallow mildly sloping foreshores: accuracy versus speed. Environ. Model. Software 130, 104740.
Longuet-Higgins, M.S., Stewart, R.W., 2006. Radiation stress and mass transport in gravity waves, with application to 'surf beats'. J. Fluid Mech. 13 (4), 481–504.
Mase, H., Tamada, T., Yasuda, T., Hedges, T.S., Reis, M.T., 2013. Wave runup and overtopping at seawalls built on land and in very shallow water. J Waterw Port Coast 139 (5), 346–357.
Oosterlo, P., Hofland, B., van der Meer, J.W., Overduin, M., Steendam, G.J., 2021. Calibration and preparation of field measurements of oblique wave run-up and overtopping on dikes using laser scanners. Coast. Eng. 167, 103915.
Owen, M., Steele, A., 1993. Effectiveness of Recurved Wave Return Walls.
Pullen, T., Liu, Y., Otinar Morillas, P., Wyncoll, D., Malde, S., Gouldby, B., 2018. A Generic and Practical Wave Overtopping Model that Includes Uncertainty. Proceedings of the Institution of Civil Engineers-Maritime Engineering, pp. 109–120.
Pullen, T., McCabe, M., Carter, D., 2012. Field and laboratory measurements of wave overtopping at anchorsholme, UK. In: Proc. 33rd Int. Conf. Coastal Engineering, Santander, ASCE.
Reniers, A., Zijlema, M., 2022. Swan surfbeat-1d. Coast. Eng. 172, 104068.
Roelvink, D., Reniers, A., van Dongeren, A., van Thiel de Vries, J., McCall, R., Lescinski, J., 2009. Modelling storm impacts on beaches, dunes and barrier islands. Coast. Eng. 56 (11–12), 1133–1152.
Romano, A., Bellotti, G., Briganti, R., Franco, L., 2015. Uncertainties in the physical modelling of the wave overtopping over a rubble mound breakwater: the role of the seeding number and of the test duration. Coast. Eng. 103, 15–21.
Salmon, J., Holthuijsen, L., 2015. Modeling depth-induced wave breaking over complex coastal bathymetries. Coast. Eng. 105, 21–35.
Sandoval, C., Bruce, T., 2018. Wave Overtopping Hazard to Pedestrians: Video Evidence from Real Accidents, Coasts, Marine Structures and Breakwaters 2017: Realising the Potential. ICE Publishing, pp. 501–512.
Saville Jr., T., 1957. Wave run-up on composite slopes. Coastal Engineering Proceedings (6), 41, 41.
Shi, F., Kirby, J.T., Harris, J.C., Geiman, J.D., Grilli, S.T., 2012. A high-order adaptive time-stepping tvd solver for boussinesq modeling of breaking waves and coastal inundation. Ocean Model. 43, 36–51.
Smit, P., Stelling, G., Roelvink, J., Van Thiel de Vries, J., McCall, R., Van Dongeren, A., Zwinkels, C., Jacobs, R., 2010. Xbeach: Non-hydrostatic Model: Validation, Verification and Model Description. Delft Univ. Technol.
Smith, L., Liang, Q., James, P., Lin, W., 2017. Assessing the utility of social media as a data source for flood risk management using a real-time modelling framework. Journal of Flood Risk Management 10 (3), 370–380.
Stockdon, H.F., Holman, R.A., Howd, P.A., Sallenger, A.H., 2006. Empirical parameterization of setup, swash, and runup. Coast. Eng. 53 (7), 573–588.
Symonds, G., Huntley, D.A., Bowen, A.J., 1982. Two-dimensional surf beat - long-wave generation by a time-varying breakpoint. J Geophys Res-Oceans 87 (Nc1), 492–498.
The SWAN Team, 2021. Swan Scientific and Technical Documentation. Swan Cycle Iii Version 41, p. 41.
Tolman, H., 1999. User manual and system documentation of wavewatch-iii version 1.18. Noaa/ncep tech, Note 166, 110.
Troch, P., Geeraerts, J., Van de Walle, B., De Rouck, J., Van Damme, L., Allsop, W., Franco, L., 2004. Full-scale wave-overtopping measurements on the zeebrugge rubble mound breakwater. Coast. Eng. 51 (7), 609–628.
Van der Meer, J.W., Nieuwenhuis, J.-W., Steendam, G.J., Reneerkens, M., Steetzel, H., van Vledder, G., 2019. Wave overtopping measurements at a real dike. Coastal Structures 2019, 1107–1117.
van der Westhuysen, A.J., 2010. Modeling of depth-induced wave breaking under finite depth wave growth conditions. J. Geophys. Res.: Oceans 115 (C1).
Yelland, M., Brown, J., Cardwell, C., Jones, D., Pascal, R., Pinnell, R., Pullen, T., Silva, E., 2022. A novel system for in-situ, wave-by-wave measurements of the speed and volume of coastal overtopping. Nature Communications. Submitted for publication.
Yuhi, M., Mase, H., Kim, S., Umeda, S., Altomare, C., 2021. Refinement of integrated formula of wave overtopping and runup modeling. Ocean Eng. 220, 108350.